Submitted to Physical Review C

LOW-ENERGY PION PRODUCTION WITH 800 MeV/N ^{20}Ne

J. Chiba, K. Nakai, I. Tanihata,
S. Nagamiya, H. Bowman, J. Ingersoll and J. O. Rasmussen

January 1979

Prepared for the U. S. Department of Energy
under Contract W-7405-ENG-48

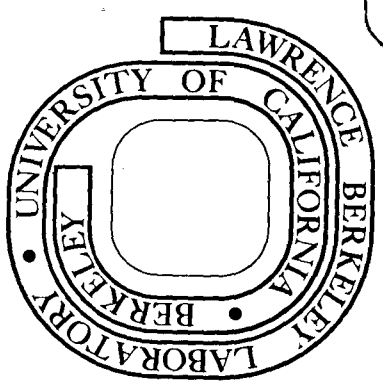

DISCLAIMER

Submitted to Physical Review C

LBL-8699
Preprint

Low-Energy Pion Production with 800 MeV/N ^{20}Ne

J. Chiba and K. Nakai

Department of Physics, University of Tokyo and
Lawrence Berkeley Laboratory, University of California

I. Tanihata

Laboratory for Nuclear Studies, Osaka University, and
Lawrence Berkeley Laboratory, University of California

and

S. Nagamiya, H. Bowman, J. Ingersoll and J. O. Rasmussen
Lawrence Berkeley Laboratory, University of California

Prepared for the U. S. Department of Energy
under Contract W-7405-ENG-48

LBL-8699

Low-Energy Pion Production with 800 MeV/N ^{20}Ne

J. Chiba and K. Nakai

Department of Physics, University of Tokyo and
Lawrence Berkeley Laboratory, University of California

I. Tanihata

Laboratory for Nuclear Studies, Osaka University, and
Lawrence Berkeley Laboratory, University of California

and

S. Nagamiya, H. Bowman, J. Ingersoll and J. O. Rasmussen
Lawrence Berkeley Laboratory, University of California

Abstract:

Doubly differential cross sections for production of positive pions (20 MeV $\leq T_\pi^{Lab} \leq$ 100 MeV) in bombardment of ^{20}Ne on NaF, Cu and Pb targets at 800 MeV/N have been measured with a range telescope. The results showed that the angular distribution of low-energy pions in the nucleon-nucleon center-of-mass ($T_\pi^{CM} \leq$ 50 MeV) was isotropic, even 90° peaking at ~15 MeV CM. The intermediate-energy pions (50 $\leq T_\pi^{CM} \leq$ 300 MeV) were forward- and backward-peaked, reflecting the individual nucleon-nucleon process in the isobar model of production. The observed cross sections were shown to be generally reproduced by an incoherent superposition of the experimental (p + nucleus) cross sections.

[NUCLEAR REACTIONS NaF, Cu, Pb(^{20}Ne, π^+)X, E/Z=800 MeV/nucleon; measured $\sigma(E_\pi, \theta_\pi)$, E_π=20-100 MeV, θ_π=30-150°.]

I. INTRODUCTION

A number of theoretical conjectures for exotic phenomena associated with high-density nuclear matter [1-3] stimulated experimental studies of high-energy nucleus-nucleus collisions. In order to search for such exotic phenomena, it is important to gain a general understanding of the basic features of high-energy heavy-ion reactions.

In the past few years, there have been more than a dozen experimental studies reported. Peripheral processes are now reasonably understood from these studies [4-6]. Studies of nonperipheral processes are now actively going on from various points of view. The streamer-chamber work by Poe et al. [7] has shown much about the peripheral and nonperipheral processes. Gosset et al. [8] reported their extensive studies on low-energy particle emissions from central-collisions and interpreted general behavior by the simple "fireball" model. Nagamiya et al. [9] have studied also central collisions, covering a much wider range of momentum distributions of emitted particles with a magnetic spectrometer. Here the data showed that the simple "fireball" model had to be modified to get a good fit, and some of the data indicated that interpretations based on individual nucleon-nucleon processes are more preferable, at least for light nuclear systems.

Models, like the "fireball," which are based on a macroscopic geometrical concept and a thermal equilibrium assumption, or hydrodynamic treatments, on the one hand, and models based on the microscopic individual nucleon-nucleon collision process, on the other hand, are the two extreme pictures for high-energy nucleus-nucleus collisions. Real processes may reflect some aspects of both extreme

models, and the validity of the models may be dependent upon projectile energies, projectile and target masses, and also upon what emitted particles are observed.

Pion production is certainly one of the important tools for investigating the reaction mechanism.

There have been several experimental studies of pion production in nucleus-nucleus collisions. Except for the earlier work by Baldin et al. [10] and Schimmerling et al. [11], most of the work was done at the Berkeley BEVALAC. Papp et al. [5] studied high-energy pions produced at forward angles by light projectiles, and showed that the pion momentum spectra could be explained by an individual nucleon-nucleus collision model taking into account the Fermi motion of nucleons in projectiles. Jakobsson et al. [12] were also able to explain their data on pion multiplicity distributions with the individual nucleon-nucleon collision model. On the other hand, the pion multiplicity data with the streamer chamber taken by Poe et al. [7] were explained with the fireball model by Gyulassy et al. [13]. Certainly more experimental studies are required to distinguish between the models. It is also of interest to look for any phenomena which are not explained by those models.

In the present work we studied the low-energy pion production in high-energy nucleus-nucleus collisions. We started this study (for $20 \leq T_{\pi}^{Lab} \leq 100$ MeV) in parallel with the work by Nagamiya et al. [9], where they measure high-energy pions ($50 \leq T_{\pi}^{Lab} \leq 1000$ MeV), so that the two experiments complement each other. Although the range we study is a tiny portion of the phase space, it covers the major part of pion yields, and thus is important to determine average multiplicities of pion production. The purpose of this measurement

is to understand low-energy pion production, particularly to facilitate extending studies further to multiple-pion triggered observations.

The low-energy pions carry unique information on the reaction. The pion absorption cross section in nuclei, empirically deduced by Sparrow et al. [14], reaches a maximum value at around $T_\pi \simeq 300$ MeV mainly due to the influence of (3,3)-resonance. It decreases monotonically as the pion energy decreases, and below 100 MeV the mean free path of pions in nuclei becomes longer than the size of nuclei. Thus the nuclei are transparent for low-energy pions. Accordingly, we note the following characteristic features:

(1) The low-energy pions produced in a nucleus-nucleus collision ("direct" pions) can easily get out of the system and would carry out direct information on the fast stage of heavy-ion reactions. We, therefore, think that the low-energy pion production probes the more violent aspects of the nucleus-nucleus collisions.

(2) There are, however, other components to the low-energy pion spectra ("secondary" pions) which are generated in secondary processes, such as "moderation" (multi-scattering) and "regeneration" (charge exchange), of high-energy pions produced in the reaction.

The low-energy pions we observe should be mixtures of the "direct" and "secondary" pions. It would be very helpful in understanding the collision process if we could find a way to distinguish between the two types of pions experimentally, or empirically in analyses.

II. EXPERIMENTAL

A. Experimental Setup

In this work we studied low-energy pion production in bombardments of the 800-MeV/N ^{20}Ne beam on NaF, Cu and Pb targets. A layout of the experimental setup is shown in Fig. 1. We used a common target position with Nagamiya and coworkers. The target was located at the center of a rotating table for a magnetic spectrometer built by Nagamiya et al. [9].

The ^{20}Ne beam from the BEVALAC was focused on the target after passing through an ion chamber for beam intensity monitoring and a multiwire ion chamber (MORGADO chamber) for monitoring beam position and size. The ion-chamber reading was recorded for every beam spill. In a series of low-intensity-beam runs, the ion-chamber current was calibrated to counting rates of a plastic scintillation counter inserted into the beam and then extrapolated for use at the higher beam intensities. In order to check linearity of the ion-chamber response, the calibration was made also with high-intensity beams by measuring ^{11}C radioactivity produced in graphite targets via ^{12}C(^{20}Ne, X)^{11}C reactions. The cross section for this reaction was estimated with an accuracy better than 30% from a set of systematic information on the ^{12}C(p,X) ^{11}C [16], ^{12}C(^{12}C,^{11}C)X [4] and ^{12}C(^{20}Ne,X) ^{11}C [17] reaction cross sections at various energies. The two calibrations agreed within the accuracies of measurements (30%).

Signals from the MORGADO chamber were displayed on an oscilloscope monitoring the beam spot throughout the run. The beam spot had to be adjusted only once or twice a day.

Three different targets, NaF, Cu and Pb, were used to study a mass dependence of the cross sections. The NaF target was chosen because the mass numbers are approximately equal to the projectile ^{20}Ne. Thicknesses of the targets were about 0.5 g/cm^2 in all the cases.

We used a pion range telescope which is described in the next section. The telescope was mounted on an arm wich was rotatable around the target independently of the magnet rotating table. The distance between target and telescope was about 50 cm. The size of a solid-angle-defining scintillator in the telescope was 5 cm x 5 cm, so that the solid angle subtended was about 10 mstr. The range of measurement covered by this telescope was 20 MeV $\leq T_\pi^{Lab} \leq$ 100 MeV and 30° $\leq \theta_\pi^{Lab} \leq$ 150.

Data were taken with a PDP 11/10 via CAMAC and stored in a magnetic tape, event by event. Adjusting the beam intensity, we kept the dead time of the data-taking system at less than 20%. The dead time was measured by counting the "Event Trigger" signals and the "Event Accepted" signals (Event trigger*Computer Busy).

B. The pion range telescope

For the detection of low-energy pions we developed a pion range telescope. Since a large number of particles of various kinds are emitted in the high energy heavy-ion reactions, it is very important to use detectors with good particle-identification capabilities. We used the $\pi^+ \rightarrow \mu^+$ decay to identify stopped π^+'s in the presence of a strong background of other particles (mostly protons). The range telescope used was a stack of plastic scintillators as shown in Fig. 2 schematically. When a π^+ comes in and stops in one of the scintillators at the position corresponding

to the range, the scintillator generates a double-pulse, one due to the π^+ followed by a delayed pulse due to the μ^+. Since the lifetime of the π^+ is short (τ_π = 26 nsec), for separation of the delayed μ^+ pulse from the prompt π^+ pulse we made fast clipping of the anode signals of phototubes (RCA 8575 or AMPEREX XP 2230), and we used fast discriminators with good pulse-pair-resolutions. The delayed pulse was taken with the fast logic circuit shown schematically in Fig. 2. A difficulty in this method was the fact that the energy of μ^+ is only 4.1 MeV. The energy deposited by the π^+ should not be too large compared to that of the μ^+. We chose the thickness of scintillator to be 1 or 2 inches. The maximum energy deposited by the π^+ in a 1-inch plastic scintillator is about 25 MeV. A time spectrum of the delayed pulses was taken for each scintillator. Although it was not possible to avoid a dead region in the time spectra of about 10 nsec, we were able to extrapolate the π^+ decay curve to t = 0. Since almost all stopped π^- are captured and disintegrate in a carbon nucleus in the scintillator, instead of decaying into μ^-, this method detects only positive pions.

The concept of range telescopes is by no means new, but combining the old method with the current sophisticated CAMAC-Computer technique we were able to make the method very powerful. In addition to the delayed time information, we recorded pulse heights of signals from all scintillators. Thus, by taking the information on the energy deposits in each plastic counter (dE/dx) along the path of a particle, we got a high degree of redundancy in identifying particles, or events. For instance, if two protons from different reaction events entered into the telescope accidentally with

a time difference of a few tens of nsec, the counter generates a double-pulse. This accidental event was a serious source of the constant background in time spectra, particularly when the telescope was set at forward angles, where more than 100 times more protons than pions passed through the telescope. However, these "background" events were easily cleaned up by use of the pulse-height information. We will discuss more technical details of the instrumentation in a separate publication.

III. RESULT

Doubly differential cross sections for the low-energy positive pion production obtained are listed in Tables 1(a) to (c) and plotted in Fig. 3. The errors shown are only statistical ones for individual numbers. Other sources of errors were uncertainties from the beam-intensity calibration and from various corrections for detection of pions, and ambiguities in subtracting background due to the beam halo hitting materials around the target. The overall uncertainties for the absolute values of the cross sections were about 30%.

For the reduction of raw data to final cross sections, the following facts were carefully checked, and necessary corrections were made:

(1) Decay in flight. The probability of the pion decay in flight was calculated for the actual geometrical arrangement. The correction factors for all scintillation counters were almost the same (~15%).

(2) Nuclear reaction. Corrections were made for the loss of pions due to nuclear reactions with nuclei in the plastic scin-

tillator (mostly the ^{12}C). This correction, however, was the largest source of uncertainties because no good cross section data for the $\pi^+ + {}^{12}C$ reaction are available for the low-energy region. We calculated the correction factor due to nuclear reactions using the empirical formula [18] of the pion-nucleus cross sections, similar to the method used in ref. [19]. It was checked also by means of an optical-model calculation [20]. Results of these two different methods were in good agreement. The typical correction factors were 10% for 60-MeV pions and 30% for 100-MeV pions.

(3) Multiple scattering and edge effects. The corrections for pions escaping from the range telescope due to multiple Coulomb scattering were calculated with the empirical formula for the deflection angle via multiple Coulomb scattering [21]. Since the telescope was designed to make the size of each element gradually larger from the front to the back, the correction factors were small (<5%).

When a pion stopped near the edge of a scintillator and the muon escaped from the counter without depositing energy above the discriminator threshold, no triggering occurred. This effect was again small (<5%). We made, however, corrections for both effects.

(4) Thickness of the target and scintillators. The measurement with the telescope was to count pions in a certain interval of energy which was determined by the thicknesses of the scintillators and the target. The energy acceptance (ΔE) and central energy for each scintillator were calculated using an empirical formula for the stopping power (dE/dx) in the plastic and the targets. Those values depend slightly on the target thickness and angle

to the direction of the detector. Typical examples are shown in Table 2.

(5) Background. In order to subtract background pions we took the data always with and without the target. The background pions observed in the run without target were considered to be mainly those from the target frame, tag counters, etc. hit by the beam halo.

IV. DISCUSSION

A. Pions from the NaF target

Since the mass numbers of Na and F are approximately equal to that of projectile ^{20}Ne, transformation of the experimental cross sections in the laboratory (LAB) frame to the center-of-mass (CM) frame is straightforward. Figure 4(a) shows a contour of the Lorenz-invariant cross sections $\frac{1}{p}(\frac{d^2\sigma}{dEd\Omega})$ in a plane of T_π^{CM}, the kinetic energy of pions in the CM frame, and θ_π^{CM}, the CM angle. Although our data do not cover the whole range of θ_π^{CM}, the plot must be symmetric about $\theta_\pi^{CM} = 90°$, permitting us to reflect data points about 90° CM as a check.

For comparison with the free nucleon-nucleon process the same plot for the ($p + p \rightarrow \pi^+ +$ anything) process at 730 MeV is shown in Fig. 4(b). The plot was made with the data by Cochran et al. [15]. For a strict comparison, we would have to include pions from the ($p + n \rightarrow \pi^+ +$ anything), but its contribution is small (~20%: $\sigma(p + n \rightarrow \pi^+ + X) = 3mb$, $\sigma(p + p \rightarrow \pi^+ + X) = 16mb$ for E = 800 MeV), and we do not make the comparison to that accuracy.

Comparing Figs. 4(a) and (b), we observe the following points:

(1) The angular and energy distribution of π^+ from the ^{20}Ne

+ NaF process is significantly different from the free nucleon-nucleon process.

(2) The intermediate energy region ($50 \leq T_\pi \leq 250$ MeV) of the distribution, however, apparently shows a marked similarity to the free nucleon process. The characteristic peak of the nucleon-nucleon collision at 180° and around 100 MeV in the center-of-mass system appears to remain.

(3) While the angular distribution is forward- and backward-peaked at higher energies ($T_\pi \geq 50$ MeV), at lower energies it is more isotropic and shows a broad peak at 90°. These facts seem to indicate that most of the intermediate-energy pions come from individual nucleon-nucleon collisions modified by Fermi motion, as in the theoretical treatment of Bertsch [22]. Clearly, there must be secondary processes, like thermalization or rescattering effects to account for the low-energy part of the distribution. The broad peak at 90° in the low-energy region (around 30 MeV) is very interesting. K. L. Wolf, A. H. Poskanzer, et al. [23] have recently reported similar observations of a low-energy 90° (CM) π^+ peak in $^{20}Ne + {}^{27}Al$ and $^{40}Ar + {}^{40}Ca$ systems at 1.0 GeV/N.

B. Comparison with a superposition of the (p + nucleus) cross section.

In order to search for effects in the pion production specific to the heavy-ion reaction, we compared our heavy-ion data with an incoherent superposition of the cross sections for the reactions, proton + nucleus → π^+ + X.

We made the simple estimate from the (p + nucleus) cross sections using the data by Cochran et al. [15], who measured the pion production cross section with 730-MeV protons on various

targets (H, D, Be, C, Al, Ti, Cu, Ag, Ta, Pb and Th). They observed pions with energies from 30 to 550 MeV at angles between 15 and 150 degrees.

Assuming no coherence among nucleons in the projectile ^{20}Ne, we calculated the cross section with the formula,

$$\left(\frac{d^2\sigma}{dEd\Omega}\right)_{Proj+T\to\pi^+ +X} = Z_{Proj}\left(\frac{d^2\sigma}{dEd\Omega}\right)_{p+T\to\pi^+ +X} + N_{Proj}\left(\frac{d^2\sigma}{dEd\Omega}\right)_{n+T\to\pi^+ +X}$$

$$= Z_{Proj}\left(\frac{d^2\sigma}{dEd\Omega}\right)_{p+T\to\pi^+ +X} + \left(\frac{Z}{N}\right)_T N_{Proj}\left(\frac{d^2\sigma}{dEd\Omega}\right)_{p+T\to\pi^+ +X}$$

where Z_{Proj}=10 and N_{Proj}=10, and T stands for the target. Because there are no data on pion-production cross sections from neutron bombardment in this energy region, the second term was replaced by the π^- production cross section from protons, assuming charge symmetry. Moreover, the factor $(Z/N)_T$ has to be multiplied to take into account the fact that the proton and neutron numbers in the target are different. This replacement is only an approximation, but we note that the contribution of the second term is much smaller than that of the first term, so that the ambiguity of the approximation does not affect the summed results so much.

Figure 5 shows a comparison between the calculated cross sections and the experimental data in the case of the Pb target. Despite the approximate nature of the expressions the agreement between calculations and experiments is rather good. In this calculation the effects of pion absorption, scattering and charge exchange in the target nucleus are included automatically by using the experimental data. Such effects in the projectile nucleus, however, are not taken into account by this calculation. Although the Fermi motion of nucleons in the projectile and the

difference of the incident energies between 730 MeV and 800 MeV/N were ignored, these effects should not be large, because the dependence on the incident energy of the pion production cross section in the nucleon-nucleon collision at this energy is weak. It may be that the lower data points, especially at 90° (lab) could arise from special shadowing effects by the projectile [23,24]. We extended the calculation to higher energy pions to compare with the data by Nagamiya et al. [25]. As shown in Fig. 6, agreement between the calculation and the experiment is very good up to 0.5 GeV/c. The data do seem to show a tail extending to higher energies than our calculation, presumably a reflection of there being neglected Fermi motion in the projectile.

V. SUMMARY

The observed angular distribution of low-energy pions in the nucleon-nucleon center-of-mass ($T_\pi^{CM} \lesssim 50$ MeV) is essentially isotropic with some peaking at 90°, while the intermediate-energy part ($50 \lesssim T_\pi^{CM} \lesssim 300$ MeV) is forward- and backward-peaked. It has been shown by Nagamiya et al. [9] that in the higher-energy region ($T_\pi^{CM} \lesssim 500$ MeV) the distribution is again isotropic.

The intermediate-energy part of the distributions appears to reflect the individual nucleon-nucleon process, and those pions are considered to be emitted from the decay of (3,3)-resonances produced (isobar model). Mandelstam gave a theoretical prediction of a $1+3\cos^2\theta$ pion angular distribution at threshold [26]. The major parts of the low-energy pions are considered to be the "secondary" pions. In particular, those in the region around

$\theta_\pi^{CM} = 90°$ (Fig. 4a) are those mostly from the central region, while around $\theta_\pi^{CM} = 0°$ or 180° there must be contributions of pions from projectiles or target fragments. The broad bump at 90° will be more pronounced if we subtract those contributions. It would be very interesting to study further the origin of those excess pions in their dependence on bombarding energy and target and projectile mass. The good agreement of the incoherent superposition of (proton + nucleus) cross sections with experiments indicated the individual nucleon-nucleon collision nature of the process for most of the pion production.

We are very grateful to the BEVALAC staff and operators for their excellent support of the experiments. We are indebted to the technical staff at Lawrence Berkeley Laboratory; G. Constantian for electronics, J. Harvill for computer hardware and many other people. Thanks are also due to Dr. M. Sasao, Miss M. Sekimoto and Mr. R. S. Hayano for their help at various stages of the experiments.

This work was supported by Nuclear Science Division of the U.S. Department of Energy under contract No. W-7405-ENG-48, and by the Mitsubishi Foundation (Japan) and the Japan Society for the Promotion of Science, and had the endorsement of the National Science Foundation.

References

[1] M. Gyulassy and W. Greiner, Z. Phys. A277, 391 (1976); A. B. Migdal, Rev. Mod. Phys. 50, 107 (1978).

[2] T. D. Lee and G. C. Wick, Phys. Rev. D9, 2291 (1974); T. D. Lee, Rev. Mod. Phys. 47, 267 (1975).

[3] A. K. Kerman and L. D. Miller, LBL-3675, 73 (1975).

[4] D. E. Greiner, P. J. Lindstrom, H. H. Heckman, Bruce Cork, and F. S. Beiser, Phys. Rev. Lett. 35, 152 (1975).

[5] J. Papp, J. Jaros, L. Schroeder, J. Staples, H. Steiner, A. Wagner and J. Wiss, Phys. Rev. Lett. 34, 601 (1975); J. Papp, Ph.D. Thesis, LBL-3633 (1975).

[6] L. Anderson, Ph.D. Thesis, LBL-6769 (1977).

[7] S. Y. Fung, W. Gorn, G. P. Kiernan, F. F. Liu, J. J. Lu, Y. T. Oh, J. Ozawa, R. T. Poe, L. Schroeder and H. Steiner, Phys. Rev. Lett. 40, 292 (1978).

[8] J. Gosset, H. H. Gutbrod, W. G. Meyer, A. M. Poskanzer, A. Sandoval, R. Stock and G. D. Westfall, Phys. Rev. C16, 629 (1977); G. D. Westfall, J. Gosset, P. J. Johansen, A. M. Poskanzer, W. G. Meyer, H. H. Gutbrod, A. Sandoval and R. Stock, Phys. Rev. Lett. 37, 1202 (1976).

[9] S. Nagamiya, I. Tanihata, S. Schnetzer, L. Anderson, W. Bruckner, O. Chamberlain, G. Shapiro and H. Steiner, Proc. Int. Conf. Nuclear Structure, Tokyo; J. Phys. Soc. Japan 44 (1978) Suppl. 378.

[10] A. M. Baldin, S. B. Garasimov, H. Guiordenescu, V. N. Zubarev, L. K. Ivanova, A. D. Kirillov, V. A. Kuznetsov, N. S. Moroz, V. B. Radomanov, V. N. Ramzhin, V. S. Stavinskii and M. L. Ytsuta, Sov. J. Nucl. Phys. 18, 91 (1974).

[11] W. Schimmerling, K. G. Vosburgh, K. Koepke and W. D. Waler, Phys. Rev. Lett. 33, 1170 (1974).

[12] B. Jakobsson, R. Kullberg, I. Otterlund, A. Ruiz, J. M. Bolta and E. Higon, Contribution to the VIIth Int. Conf. on High-energy Physics and Nuclear Structure (Zurich, Aug. 29 - Sept. 2, 1977).

[13] M. Gyulassi and S. K. Kauffmann, Phys. Rev. Lett. 40, 298 (1978).

[14] D. A. Sparrow, M. M. Sternheim and R. R. Silbar, Phys. Rev. C10, 2215 (1974).

[15] D. R. F. Cochran, P. N. Dean, P. A. M. Gram, E. A. Knapp, E. R. Martin, D. E. Nagle, P. B. Perkins, W. J. Shlaer, H. A. Thiessen and E. D. Theriot, Phys. Rev. D6, 3085 (1972).

[16] J. B. Cumming, Ann. Rev. Nucl. Sci. 13, 260 (1963).

[17] A. R. Smith and R. H. Thomas, LBL-3861 (1975).

[18] C. Richard-Serre and M. J. M. Saltmarsh, Nucl. Inst. Meth. 63, 173 (1968).

[19] P. W. James, D. A. Bryman, G. R. Mason, L. P. Robertson, T. R. Witten and J. S. Vincent, TRIUMF Rep. TRI-PP-76-3 (1976).

[20] M. Sasao, private communication.

[21] Particle Properties Booklet, CERN, p. 72 (1976).

[22] G. F. Bertsch, Phys. Rev. C15, 713 (1977).

[23] K. L. Wolf et al., Bull. Am. Phys. Soc. 23, 959 (1978), Abstract FB 10.

[24] J. Sullivan and J. O. Rasmussen, Bull. Am. Phys. Soc. 23, 956 (1978), Abstract EE 11.

[25] S. Nagamiya et al., unpublished data.

[26] S. Mandelstam, Proc. Roy. Soc. London 244, 491 (1958).

Table 1(a). Cross section for π^+ from NaF in μb/sr/MeV. (Numbers in parentheses are uncertainties.)

Pion energy T_π^{Lab} (MeV)	Angle θ_π^{Lab} (Degree)					
	30	45	58	90	120	150
19	113 (10)	87 (6)	79 (6)	87 (6)	134 (6)	125 (7)
29	113 (10)	124 (8)	98 (7)	113 (6)	152 (6)	136 (6)
40	165 (13)	151 (9)	127 (7)	137 (6)	165 (6)	151 (6)
49	189 (15)	193 (10)	138 (8)	145 (7)	169 (6)	146 (6)
61	---	189 (10)	166 (8)	137 (6)	158 (5)	114 (6)
72	186 (18)	207 (11)	158 (9)	115 (6)	123 (7)	90 (7)
83	212 (18)	220 (13)	154 (11)	110 (9)	102 (7)	75 (5)
93	190 (18)	211 (13)	152 (10)	90 (8)	79 (5)	45 (5)
102	228 (24)	218 (16)	128 (12)	76 (10)	56 (7)	26 (8)

Table 1(b). Cross section for π^+ from Cu in μb/sr/MeV. (Numbers in parentheses are uncertainties.)

Pion energy T_π^{Lab}(MeV)	Angle θ_π^{Lab} (Degree)					
	30	45	58	90	120	150
19	202 (29)	188 (19)	194 (16)	196 (9)	259 (13)	208 (20)
29	235 (23)	208 (20)	220 (17)	256 (10)	327 (13)	261 (16)
40	255 (31)	264 (22)	314 (19)	317 (12)	358 (13)	281 (18)
49	333 (36)	318 (24)	350 (20)	327 (12)	356 (14)	275 (18)
61	---	390 (22)	371 (16)	301 (10)	260 (15)	233 (16)
72	309 (45)	314 (26)	364 (20)	249 (17)	239 (16)	157 (16)
83	309 (39)	356 (32)	349 (28)	232 (18)	224 (12)	103 (15)
93	231 (40)	361 (30)	313 (22)	189 (13)	151 (13)	100 (14)
102	246 (55)	295 (33)	300 (28)	177 (17)	132 (13)	56 (9)

Table 1(c). Cross section for π^+ from Pb in μb/sr/MeV. (Numbers in parentheses are uncertainties.)

Pion energy T_π^{Lab}(MeV)	Angle θ_π^{Lab} (Degree)					
	30	45	58	90	120	150
19	310 (62)	386 (40)	279 (36)	248 (25)	391 (29)	412 (27)
29	340 (42)	401 (35)	333 (26)	310 (20)	567 (23)	532 (25)
40	616 (62)	447 (53)	442 (28)	468 (24)	621 (28)	617 (37)
49	656 (67)	592 (48)	503 (37)	474 (27)	674 (26)	602 (29)
61	---	623 (42)	513 (35)	450 (24)	624 (24)	534 (25)
72	631 (79)	570 (56)	508 (40)	413 (34)	477 (34)	417 (29)
83	602 (81)	686 (60)	531 (37)	417 (20)	403 (32)	316 (25)
93	613 (75)	502 (58)	397 (38)	287 (28)	323 (26)	216 (20)
102	606 (95)	569 (69)	448 (47)	231 (32)	229 (27)	178 (22)

Table 2. Energy acceptance and mean energy of pion stopped in each element of the telescope (in unit of MeV). *

	(a)		(b)		(c)	
Element	Mean energy	Energy acceptance	Mean energy	Energy acceptance	Mean energy	Energy acceptance
R_1	18.5	8.1	19.7	7.8	19.3	7.9
R_2	28.5	12.0	29.4	11.8	29.2	11.8
R_3	39.4	9.8	40.2	9.7	40.0	9.7
R_4	48.7	8.7	49.3	8.6	49.1	8.6
R_5	60.8	15.5	61.4	15.5	61.2	15.5
R_6	72.1	7.2	72.6	7.2	72.5	7.2
R_7	82.5	13.6	83.0	13.5	82.9	13.6
R_8	92.5	6.5	93.0	6.5	92.9	6.5
R_9	102.0	12.6	102.5	12.6	102.4	12.6

* These values depend on the target thickness and angle to the detector direction. Here, three typical examples are listed; in columm a) without taking into account the target thickness, b) with the NaF target at 60 degree to the detector, and c) with the Pb target at the same angle.

Figure Captions

Fig. 1. Schematic diagram of the experimental setup. The target angle to the beam was changed depending on the detector angle.

Fig. 2. A schematic diagram of the range telescope, thicknesses, and sizes of the plastic scintillators, and a schematic drawing of the electronic circuit for detecting pion decays.

Fig. 3. Doubly differential cross sections for positive pion production with the 800 MeV/N ^{20}Ne beam on (a) NaF, (b) Cu, and (c) Pb targets, respectively. The errors are only statistical ones.

Fig. 4. Contour plots of the Lorentz-invariant cross sections (a) for $^{20}Ne + NaF \rightarrow \pi^+ +$ anything at 800 MeV/N, and (b) for $p + p \rightarrow \pi^+ +$ anything at 730 MeV [15]. The numbers written along with the contour lines are invariant cross sections in unit of $mb/sr^{-1}(GeV)^{-1}\cdot c$. The black dots indicate the observed points. The contour lines should be symmetric about $\theta_\pi^{CM} = 90°$.

Fig. 5. Comparison of the experimental cross section (black dots) for $^{20}Ne + Pb \rightarrow \pi^+ +$ anything with the calculation based on the incoherent superposition of the cross sections for $p + Pb \rightarrow \pi^\pm +$ anything.

Fig. 6. Comparison of the calculated cross sections with experimental results by Nagamiya et al. [22] for higher-energy pions.

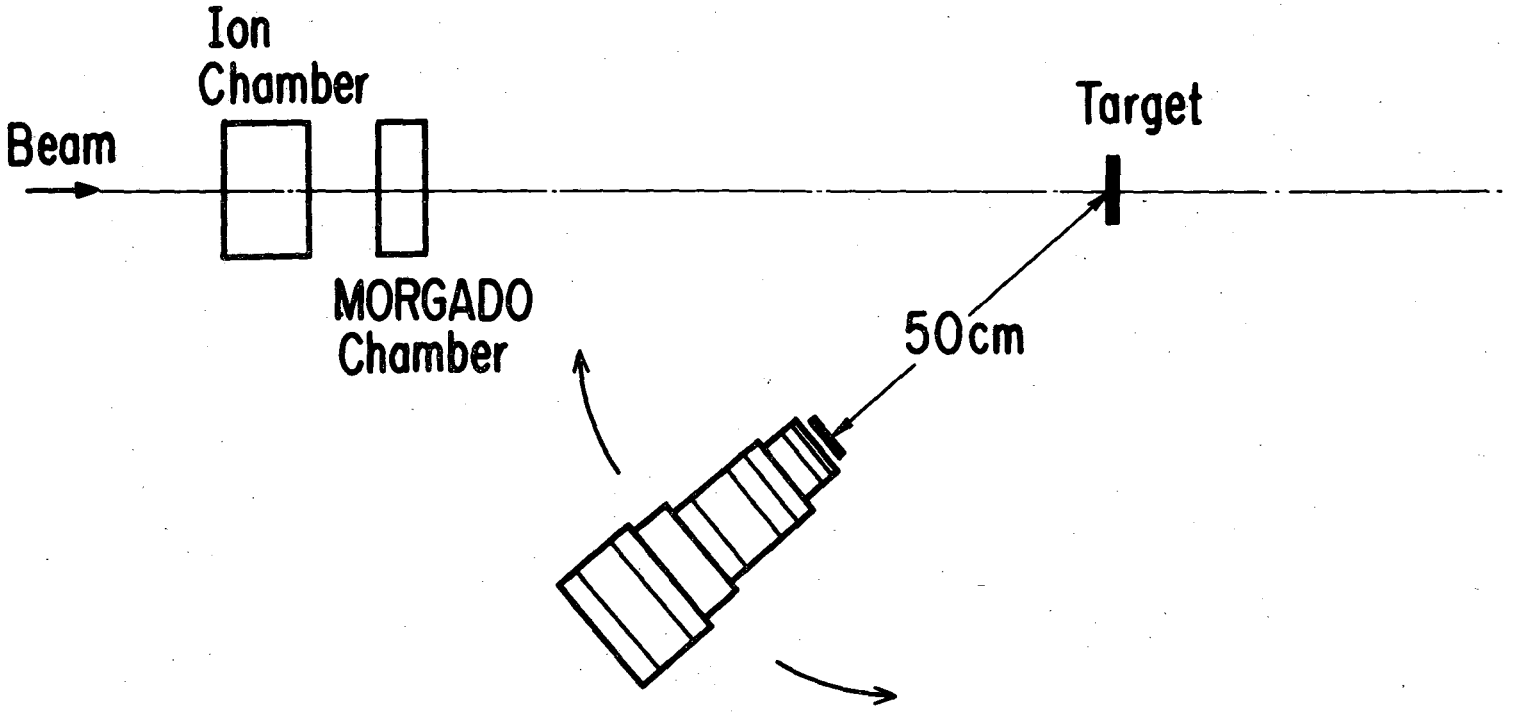

XBL 7812-14100

Fig. 1

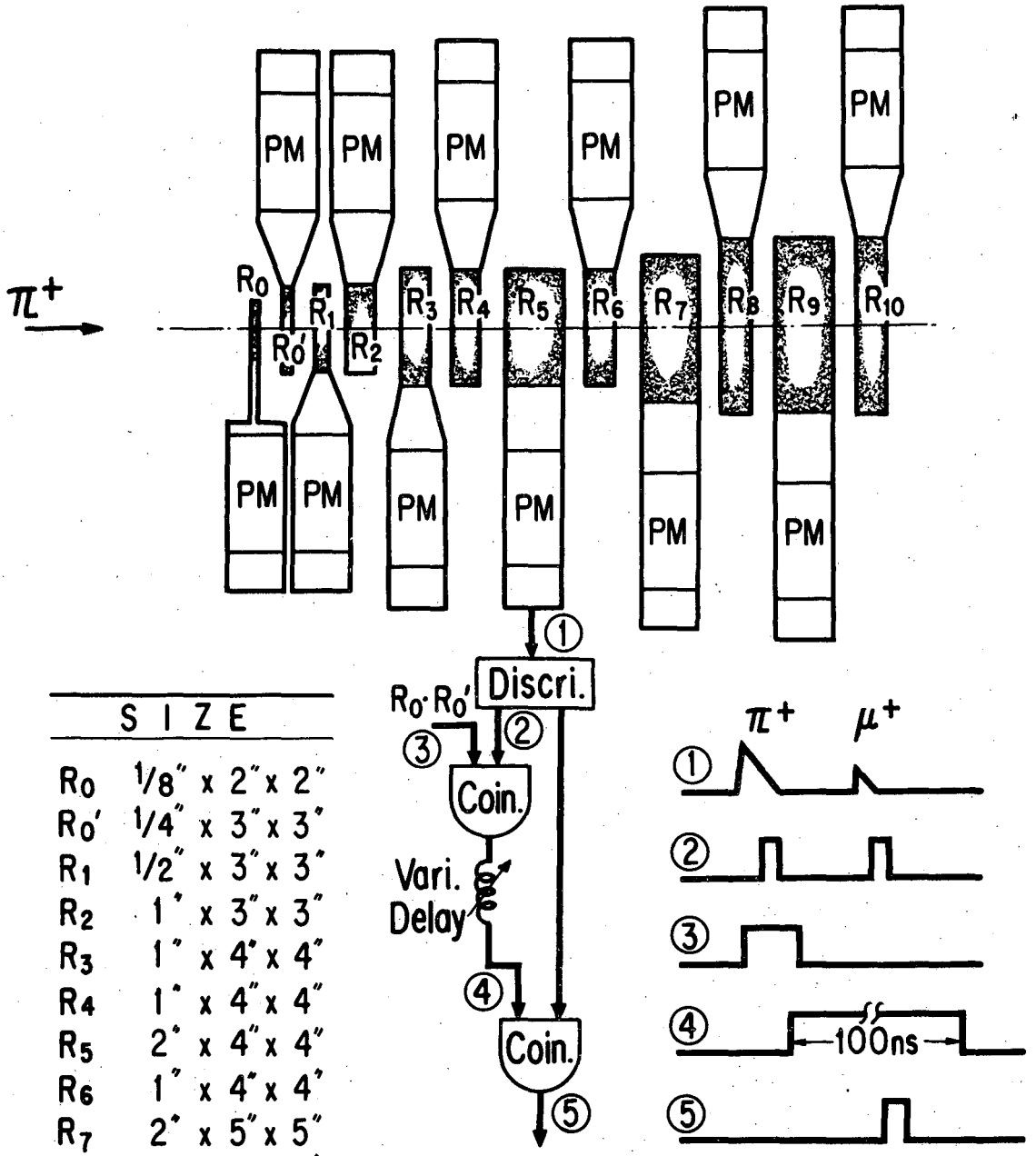

SIZE	
R_0	1/8" x 2" x 2"
R_0'	1/4" x 3" x 3"
R_1	1/2" x 3" x 3"
R_2	1" x 3" x 3"
R_3	1" x 4" x 4"
R_4	1" x 4" x 4"
R_5	2" x 4" x 4"
R_6	1" x 4" x 4"
R_7	2" x 5" x 5"
R_8	1" x 6" x 6"
R_9	2" x 6" x 6"
R_{10}	1" x 6" x 6"

XBL 7812-14101

Fig. 2

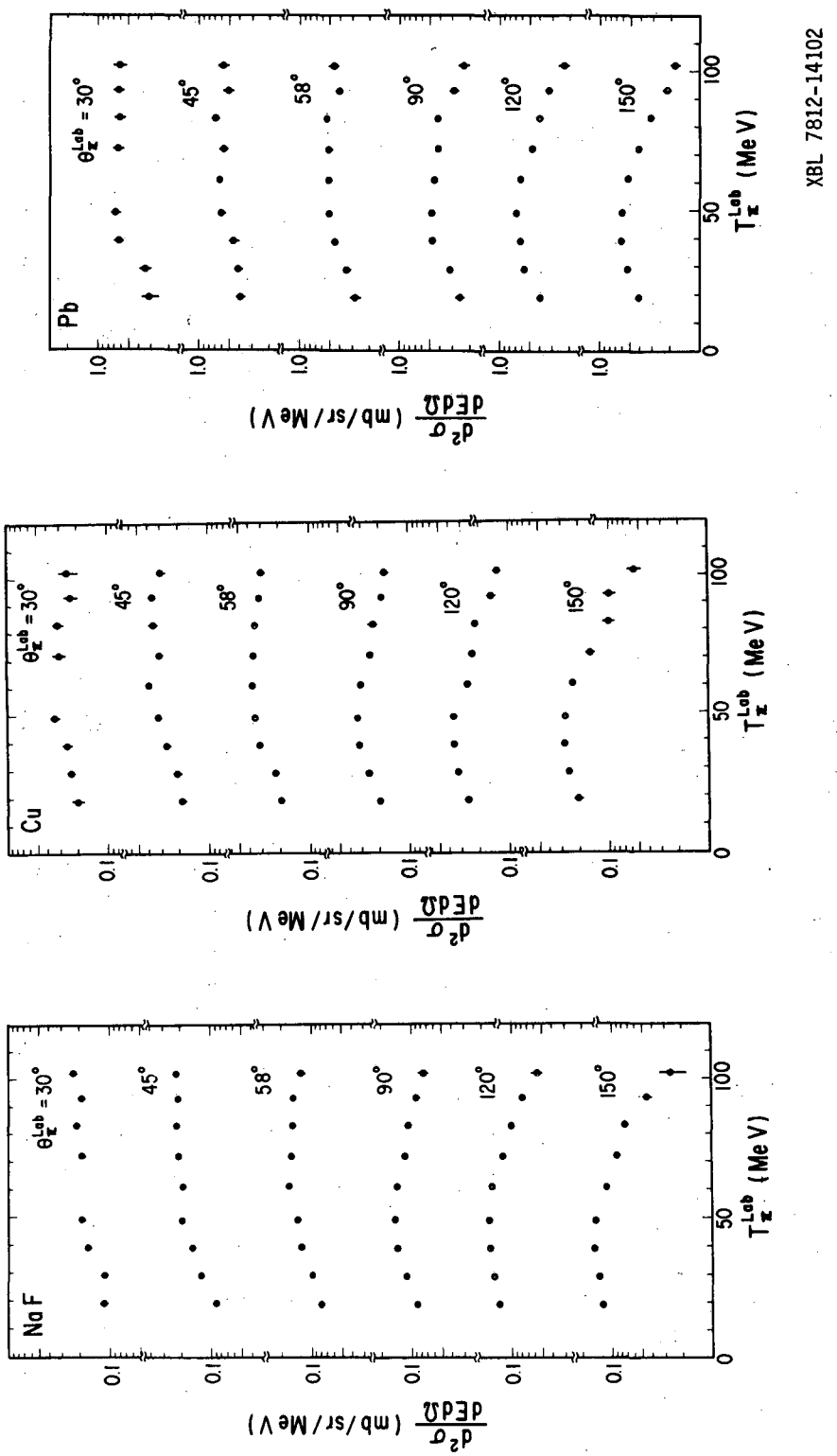

XBL 7812-14102

Fig.3

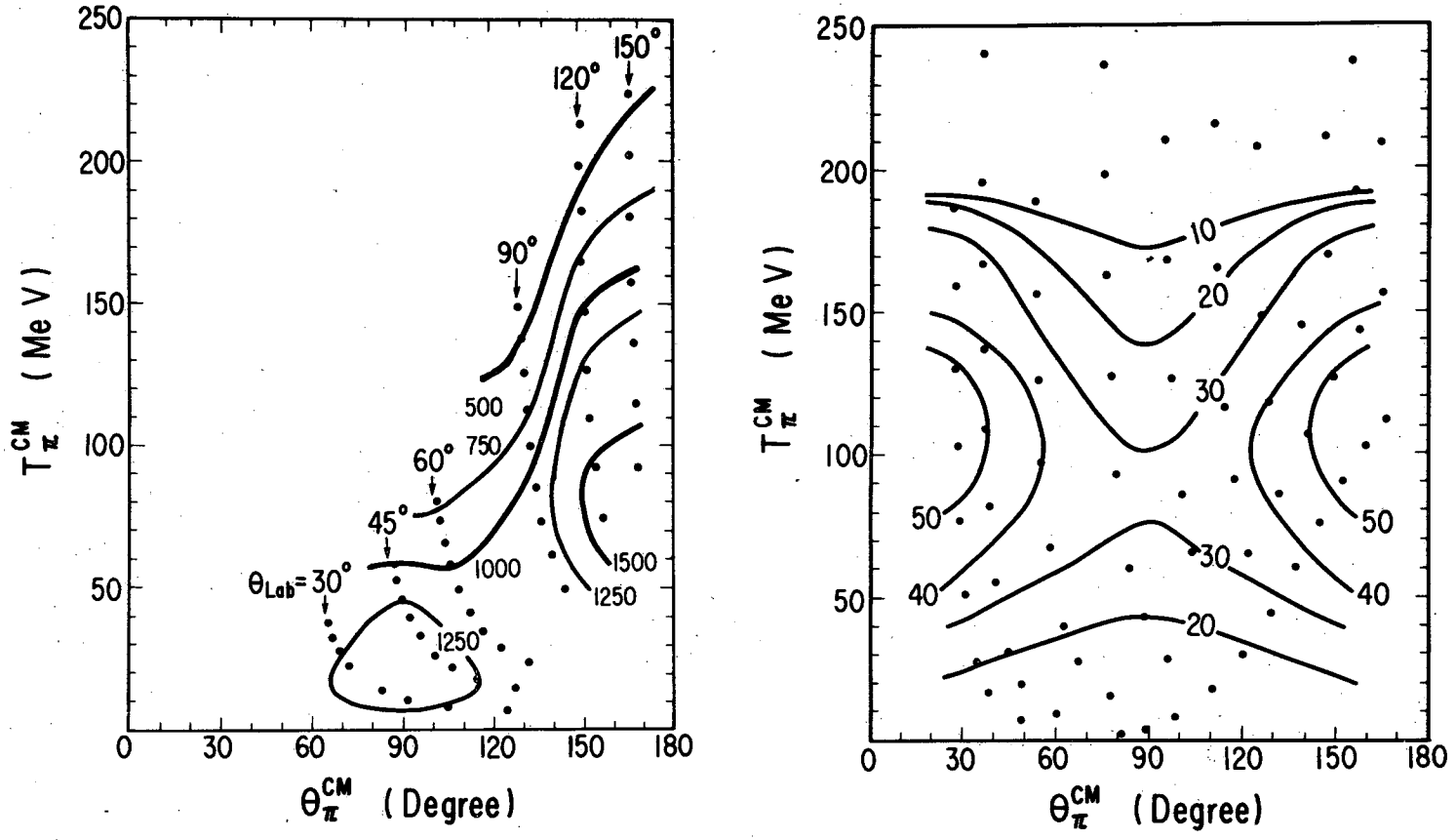

XBL 7812-14103

Fig. 4

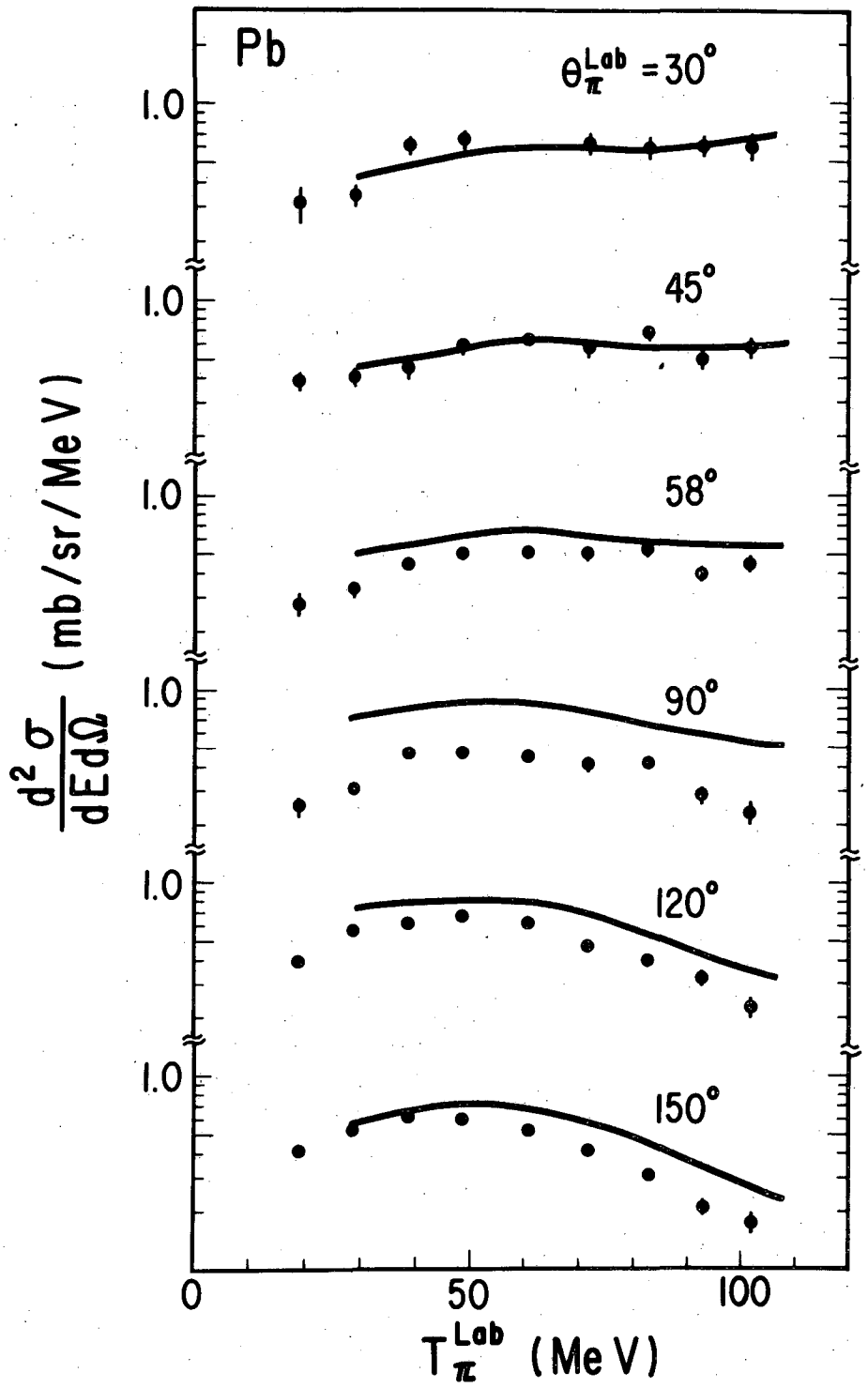

XBL 7812-14104

Fig. 5

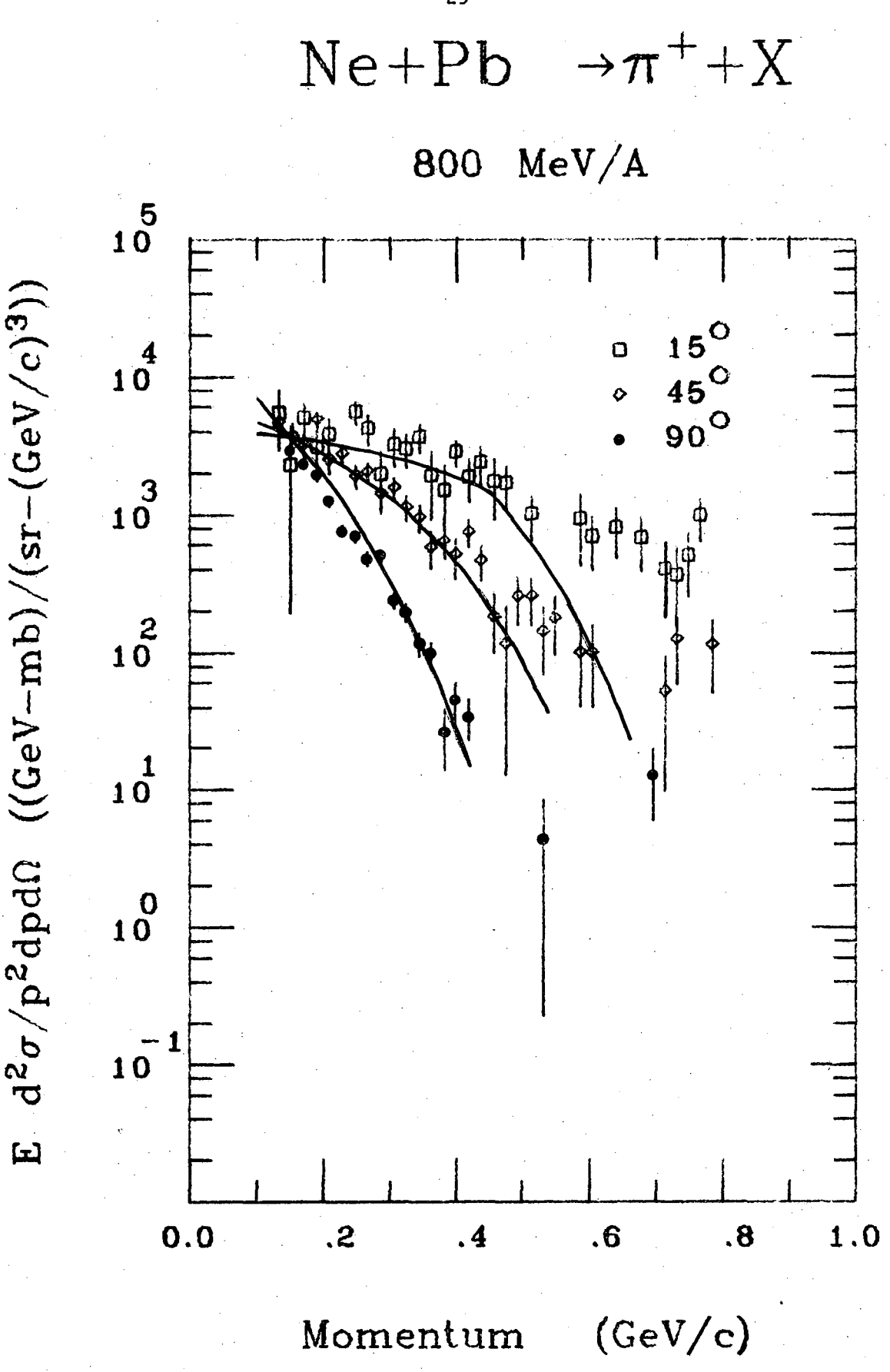
Ne+Pb →π⁺+X
800 MeV/A
E d²σ/p²dpdΩ ((GeV-mb)/(sr-(GeV/c)³))
10⁵
10⁴
10³
10²
10¹
10⁰
10⁻¹
15°
45°
90°
0.0
.2
.4
.6
.8
1.0
Momentum (GeV/c)
XBL 791-7787

Fig. 6

This report was done with support from the Department of Energy. Any conclusions or opinions expressed in this report represent solely those of the author(s) and not necessarily those of The Regents of the University of California, the Lawrence Berkeley Laboratory or the Department of Energy.

Reference to a company or product name does not imply approval or recommendation of the product by the University of California or the U.S. Department of Energy to the exclusion of others that may be suitable.

TECHNICAL INFORMATION DEPARTMENT
LAWRENCE BERKELEY LABORATORY
UNIVERSITY OF CALIFORNIA
BERKELEY, CALIFORNIA 94720